JOURNAL OF SYNCHROTRON RADIATION
ISSN 1600-5775

Detective quantum efficiency for photon-counting hybrid pixel detectors in the tender X-ray domain: application to Medipix3RX

Jean Rinkel,* Debora Magalhães, Franz Wagner, Florian Meneau and Flavio Cesar Vicentin

Brazilian Synchrotron Light Laboratory, CNPEM, Rua Giuseppe Máximo Scolfaro 10.000, Caixa Postal 6192, Campinas, SP 13083-970, Brazil. *Correspondence e-mail: jean.rinkel@lnls.br

Received 28 August 2015
Accepted 26 October 2015

Edited by S. Svensson, Uppsala University, Sweden

Keywords: Medipix3RX; tender X-rays; detective quantum efficiency.

Synchrotron-radiation-based X-ray imaging techniques using tender X-rays are facing a growing demand, in particular to probe the *K* absorption edges of low-*Z* elements. Here, a mathematical model has been developed for estimating the detective quantum efficiency (DQE) at zero spatial frequency in the tender X-ray energy range for photon-counting detectors by taking into account the influence of electronic noise. The experiments were carried out with a Medipix3RX ASIC bump-bonded to a 300 µm silicon sensor at the Soft X-ray Spectroscopy beamline (D04A-SXS) of the Brazilian Synchrotron Light Laboratory (LNLS, Campinas, Brazil). The results show that Medipix3RX can be used to develop new imaging modalities in the tender X-ray range for energies down to 2 keV. The efficiency and optimal DQE depend on the energy and flux of the photons. The optimal DQE values were found in the 7.9–8.6 keV photon energy range. The DQE deterioration for higher energies due to the lower absorption efficiency of the sensor and for lower energies due to the electronic noise has been quantified. The DQE for 3 keV photons and 1×10^4 photons pixel^{-1} s^{-1} is similar to that obtained with 19 keV photons. Based on our model, the use of Medipix3RX could be extended down to 2 keV which is crucial for coming applications in imaging techniques at modern synchrotron sources.

1. Introduction

Synchrotron-radiation-based X-ray imaging techniques using tender X-rays (from 1500 to 4500 eV) are facing a growing demand due to the many advantages that have already been identified, such as higher X-ray fluxes, higher coherent areas and better speckle resolution for coherent diffraction techniques, and the possibility to image simultaneously different harmonics of the beam. However, many difficulties still remain. Indeed, these new techniques are facing the challenges of designing beamline attenuators presenting high attenuation of tender X-rays for most materials and X-ray detectors enabling a good discrimination between the signals due to the X-ray photons and to the electronic noise.

The future 3 GeV Brazilian synchrotron light source, SIRIUS, is designed to have an ultra-low emittance (0.28 nm rad), high brightness and high spatial coherence, opening new perspectives for research, particularly in the tender X-ray energy range. Simulations of the brilliance of the future SIRIUS synchrotron can be found in Liu *et al.* (2013). Two beamlines have been particularly designed to be optimized for tender X-rays: CARNAUBA (Coherent X-ray Nanofocus beamline) is the scanning tender/hard X-ray nanoprobe beamline; CATERETÊ (Coherent and Time-Resolved

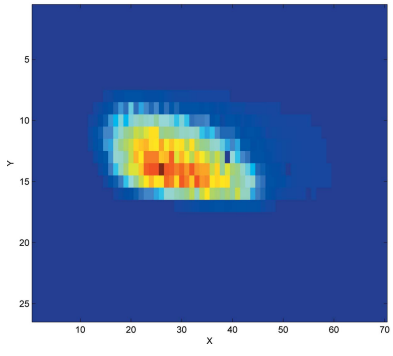

Scattering beamline) will provide unique capabilities in biological and soft materials imaging and dynamics experiments with particular focus on the application of coherent X-ray scattering and diffraction techniques. Coherent X-ray diffractive imaging (CXDI) and X-ray photon correlation spectroscopy (XPCS) experiments will be at the heart of the activities planned at this beamline, but also time-resolved small-angle X-ray scattering, which will benefit from the high flux of the source.

The principal scientific motivation in the tender X-ray energy range is the possibility to study electronic and atomic structure of low-Z elements by probing their K absorption edges. It is especially interesting for biological studies since the K-edges of the main elements of interest, such as phosphorus (2.145 keV), sulfur (2.472 keV), chlorine (2.822 keV), potassium (3.608 keV) or calcium (4.0379 keV), can be reached. By tuning the beam energy around these absorption edges, one could extract not only structural information about the biological specimens but also correlate it with the oxidation state of these chemical elements. An optimal energy around tender X-ray energies at 2.5 keV was reported in phase-contrast X-ray microscopy of large eukaryotic cells, by considering specimen size, radiation dose and depth-of-focus (Wang *et al.*, 2013).

Moreover, for techniques requiring coherent radiation, such as plane-wave coherent diffraction imaging (pwCDI), Bragg CDI, ptycography (Miao *et al.*, 2015) and X-ray photon correlation spectroscopy, or XPCS (Shpyrko, 2014), the transverse coherence lengths are proportional to the wavelength and then the photon flux transmitted by the coherent area of the beam varies with λ^2 (van der Veen & Pfeiffer, 2004):

$$F = B\lambda^2 \frac{\Delta\lambda}{\lambda}, \quad (1)$$

where B is the brilliance of the source. In conclusion, the tender X-ray range offers the possibility to increase the size of the object to be imaged.

For conventional small-angle X-ray scattering, we can reach lower q values with the same distance between sample and detector and the same detector geometry. This implies a better speckle resolution in coherent diffraction imaging. Finally, another advantage is the possibility to perform simultaneous measurements of first and third harmonics, for example in the case of 111 or 311 silicon monochromators.

Hybrid silicon photon-counting detectors can meet the requirements of very high dynamic range and high detection efficiency especially needed for imaging applications using synchrotron radiation. Compared with other families of hybrid pixel detectors, such as Pilatus (Kraft *et al.*, 2009) and XPAD (Pangaud *et al.*, 2008), the Medipix3RX photon-counting pixel readout chip enables a higher spatial resolution with a pixel size of 55 µm by 55 µm. Furthermore, this chip takes advantage of the 130 nm CMOS technology to allow a high level of functionality in each pixel. The main novel feature of Medipix3RX is inter-pixel communication. By summing together the signals from neighbouring pixels at a series of 'summing nodes', and assigning each hit to the node with the highest signal, the chip can compensate for charge-sharing effects (Pennicard *et al.*, 2011). Medipix3RX was characterized for energies between 6 and 15 keV (Frojdh *et al.*, 2014) in terms of dead-time and energy resolution. Medipix3RX characterization at low energies is a fundamental step to develop new tender X-ray imaging techniques for synchrotron applications. This is crucial for optimizing the beamline design of new imaging techniques (pwCDI, ptychography, Bragg CDI, XPCS) using a counting detector. However, counting detectors can detect individual photon hits within a user-defined energy range, making it possible to achieve virtually noise-free X-ray images. For this reason, the already published methods to evaluate the image quality on counting detectors do not consider the influence of the electronic noise (Marchal & Medjoubi, 2012; Michel *et al.*, 2006; Ponchut, 2006; Wernecke *et al.*, 2014). The study of Wernecke *et al.* (2014) presents similarities with the current work since it focuses on characterization of the in-vacuum Pilatus detector at low energies, down to 1.75 keV. The main difference is that the thresholds are kept to values higher than the noise floor with a 1.7 keV lower bound, to ensure that the electronic noise remains negligible. Our approach enables a more complex fine optimization of the threshold by allowing false counts due to electronic noise.

In this paper we describe a generalization of the model proposed by Michel *et al.* (2006) including the influence of electronic noise on the detective quantum efficiency (DQE) at zero spatial frequency. Experimental results were obtained at the Soft X-ray Spectroscopy beamline of the UVX Brazilian synchrotron. We show results of DQE combining experimental data and the original DQE model.

2. Material and methods

2.1. SXS beamline

Low-energy characterization with the Medipix3RX detector was carried out using the Soft X-ray Spectroscopy beamline (D04A-SXS) at the Brazilian Synchrotron Light Laboratory (LNLS, Campinas, Brazil). The LNLS storage ring operates with an electron energy of 1.37 GeV, natural emittance of 100 nm rad and a critical energy of 2.08 keV. The SXS beamline photon energy ranges from 800 to 5500 eV, and synchrotron radiation is generated by a bending-magnet source, focused at the sample position by a Ni-coated toroidal mirror and monochromated by a double-crystal monochromator equipped with four different crystals, InSb(111), Si(111), YB_{66}(400) and beryl(10−10). In this experiment, Si(111) double crystals were used to set the beam to the following energies for Medipix3RX detector characterization: 2, 2.25, 2.5, 2.75, 3, 4 and 5 keV. The energy scale was calibrated with a molybdenum metallic foil, using the Mo L_3-edge at 2520 eV.

Detuning of the double-crystal X-ray monochromator was used to suppress higher-order harmonics in the monochromatic beam. The intensity loss due to detuning varied between

50% and 90%, giving a monochromatic intensity at the detector position between 6×10^6 and 1×10^8 photons s^{-1}, depending on the photon energy. Details of the commissioning results of the beamline have been published in the literature (Abbate *et al.*, 1999).

For energies under 5 keV, the beamline must work under ultra-high vacuum conditions. Due to the intrinsic high photon absorption characteristics of available window materials, no isolating windows between the storage ring and beamline are normally used. However, Medipix3RX was used at atmospheric pressure and room temperature for the current experiments. In order to fulfill this condition and, at the same time, to preserve the beamline vacuum integrity in case of eventual leakage, the experimental setup included a differential pumping system with two capillary stages and a 100 µm beryllium exit window.

2.2. Experimental setup

Measurements were performed with a Medipix3RX ASIC bump-bonded to a 300 µm silicon sensor. The chip was used in conventional single-pixel mode configured with 24-bit counters per pixel (Gimenez *et al.*, 2011). The detector was read out using the *Fitpix* USB interface for Medipix3RX and *Pixelman* software, both developed by the Institute of Experimental and Applied Physics (IEAP) in Prague (Vykydal *et al.*, 2006). SXS beam spectra were acquired by scanning Medipix3RX low-energy threshold using 2, 2.25, 2.5, 2.75, 3, 4 and 5 keV beams. Medipix3RX was used in super high gain mode (SHGM) to optimize the detection of low-energy photons.

2.3. Data processing

2.3.1. Fraction of counted photons. The fraction of incident photons that are counted depends on the analog threshold, which is set as a function of the acceptable level of electronic noise. This acceptable level of electronic noise is expressed as a mean number of false counts per pixel per second. In this section the charge sharing effect is not taken into account. Thus we considered only the incident photons which interacted without charge sharing. The detector is irradiated by a monochromatic beam at energy E_0. The energy resolution of the detector is denoted FWHM (full width at half-maximum) and the energy dispersion is supposed to be Gaussian. By scanning the threshold and calculating the first derivative of the signal we obtain the incident beam spectrum. The energy resolution is calculated by fitting the measured differential spectrum by a Gaussian distribution for threshold values corresponding to energies higher than E_0 to limit the influence of charge-sharing effects. We can deduce the fraction of counted photons for the photons without charge sharing, F, as a function of the energy of the threshold, denoted $E_{\rm th}$:

$$F = \frac{1}{2}\left[1 + \mathrm{erf}\left(\frac{E_0 - E_{\rm th}}{\mathrm{FWHM}/\{2[\ln(2)]^{1/2}\}}\right)\right]. \quad (2)$$

Fig. 1 shows the differential number of events counted per pixel and per second as a function of the threshold for a 3 keV beam, without X-ray photons (noise scan) and the curve

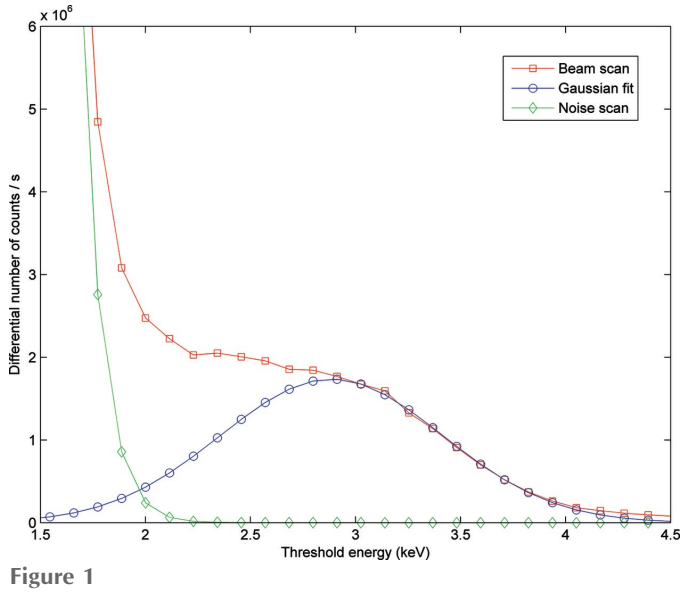

Figure 1
Differential scans with 3 keV photons, without photons (Noise scan) and Gaussian fit. Medipix3RX was configured in super high gain mode.

obtained by a Gaussian fit for threshold values corresponding to energies higher than 3 keV.

2.3.2. Model of DQE. The DQE is a commonly used figure of merit to quantify the noise performance of an imaging system, generally expressed as a function of spatial frequency. It can be defined as the square of the measured signal-to-noise ratio, $\mathrm{SNR}_{\rm out}$, divided by the incident signal-to-noise ratio, $\mathrm{SNR}_{\rm in}$:

$$\mathrm{DQE} = \mathrm{SNR}^2_{\rm out}/\mathrm{SNR}^2_{\rm in}. \quad (3)$$

In a former study, Michel *et al.* (2006) proposed a method to quantify the quantum efficiency (DQE) at zero spatial frequency for a photon-counting detector. For most applications the threshold level is set up above the noise floor and electronic noise is neglected. For fine optimization of image quality at low energies (tender X-rays) we needed to generalize the model proposed by Michel *et al.* to include the influence of electronic noise on the DQE at zero spatial frequency.

Following Michel's methodology, we can express the measurements as a sum of single counts N_1, double counts N_2 and so on.

$$N_{\rm meas} = N_1 + 2N_2 + \ldots = \sum_{i=1}^{\infty} iN_i. \quad (4)$$

This measurement is obtained by subtracting the false counts due to the electronic noise $N_{\rm noise}$ from the raw data.

The number of detected X-ray photons is

$$N_{\rm true} = N_1 + N_2 + \ldots = \sum_{i=1}^{\infty} N_i. \quad (5)$$

Assuming statistical independence between the variables N_i and the electronic noise, we can express the variance of the measured counting value as a function of the electronic noise variance, denoted $\sigma^2_{\rm Noise}$:

$$\sigma^2_{N_{\rm meas}} = \sum_{i=1}^{\infty} i^2 N_i + \sigma^2_{\rm Noise}. \quad (6)$$

The measured signal-to-noise ratio is given by:

$$\mathrm{SNR}_{\rm out} = \frac{\sum_{i=1}^{\infty} iN_i}{\left(\sum_{i=1}^{\infty} i^2 N_i + \sigma^2_{\rm Noise}\right)^{1/2}}. \quad (7)$$

The incident SNR is:

$$\mathrm{SNR}_{\rm in} = \sqrt{N_{\rm in}}. \quad (8)$$

Finally, we obtain an expression of the detective quantum efficiency (DQE) at zero spatial frequency from equations (3), (7) and (8):

$$\mathrm{DQE} = \frac{\left(\sum_{i=1}^{\infty} iN_i\right)^2}{N_{\rm in}\left(\sum_{i=1}^{\infty} i^2 N_i + \sigma^2_{\rm Noise}\right)}. \quad (9)$$

We introduce now the averaged multiplicity per detected photon:

$$\langle m\rangle = \frac{N_{\rm meas}}{N_{\rm true}}. \quad (10)$$

The average quadratic multiplicity is defined by:

$$\langle m^2\rangle = \frac{\sum_{i=1}^{\infty} i^2 N_i}{N_{\rm true}}. \quad (11)$$

Let us introduce the detection efficiency:

$$\varepsilon = \frac{N_{\rm true}}{N_{\rm in}}. \quad (12)$$

Combining equations (9)–(11), we propose a new expression for the detective quantum efficiency at zero spatial frequency:

$$\mathrm{DQE} = \frac{\langle m\rangle^2 \varepsilon N_{\rm in}}{N_{\rm in}\langle m^2\rangle + \left(\sigma^2_{\rm Noise}/\varepsilon\right)}. \quad (13)$$

The equation given by Michel *et al.* is recovered when neglecting the electronic noise ($\sigma^2_{\rm Noise} = 0$):

$$\mathrm{DQE} = \frac{\langle m\rangle^2}{\langle m^2\rangle}\,\varepsilon. \quad (14)$$

Let us detail the expression of ε as a function of measurable parameters (the description on how they are determined can be seen in the following section). The detection efficiency is affected by two phenomena: the absorption of the photons by the sensor, denoted a, with $a \in [0, 1]$, and the missing photons due to the energy threshold. P is the probability of charge-sharing for an absorbed photon, defined as the probability for an X-ray of not depositing fully its energy in one pixel. We have then:

$$N_{\rm in} = \frac{N_1}{(1-P)\,a}. \quad (15)$$

Finally,

$$\varepsilon = \frac{N_{\rm meas}}{N_1}\,\frac{(1-P)\,a}{\langle m\rangle}. \quad (16)$$

2.3.3. Determination of DQE parameters in single-pixel mode. The objective of this section is to propose a method to estimate the parameters of the proposed model to quantify the DQE of Medipix3RX in single-pixel mode.

The number of photons N_1 which interact without charge-sharing can be deduced from monochromatic measurements by fitting the spectrum for thresholds values corresponding to energies higher than the beam energy. The area under the Gaussian is an estimation of N_1.

The absorption a is deduced from an X-ray attenuation database (Henke *et al.*, 1993) by considering the sensor material and thickness (300 µm of Si for this study) and the energy of the X-ray photons.

$N_{\rm in}$ is measured by using the charge summing mode of Medipix3RX (Pennicard *et al.*, 2011). This feature of the Medipix3 photon-counting pixel readout chip is based on inter-pixel communication. By summing together the signals from neighbouring pixels at a series of 'summing nodes', and assigning each hit to the node with the highest signal, the chip can compensate for charge-sharing effects. The integral value of an energy threshold scan in charge summing mode is an estimation of $N_{\rm in}\,a$.

The average multiplicity $\langle m\rangle$ and its fluctuations $\langle m^2\rangle$ can be calculated using the method proposed by Michel *et al.* (2006) using low-flux images and analysing the size of the clusters of pixels corresponding to each detected photon. Actually, it is well established that for thresholds corresponding to energies higher than half of the photon energy ($E_0/2$) the multiplicity is 1. For these threshold values, the spatial resolution is kept at an optimal value (each absorbed photon is counted once in one pixel). For this reason, the optimizations of DQE are performed in the [$E_0/2$, E_0] energy range, assuming $\langle m\rangle = 1$ and $\langle m^2\rangle = 1$.

The noise variance $\sigma^2_{\rm Noise}(th)$ is calculated by analysing the images obtained without detector irradiation with different threshold values *th*.

3. Results

3.1. Fraction of counted photons

Figs. 2 and 3 show the image of the SXS beam at 2 keV and its vertical and horizontal integrated profiles, respectively. To distinguish between X-ray photons and electronic noise, the threshold value was fixed to 2.2 keV, resulting in a good noise rejection (45 false counts *versus* up to 2.1×10^5 photons counted per pixel in 10 s) but a very poor efficiency (estimated to be 35%). These false counts are not visible in Fig. 2 since the linear scale ranges from 0 to 2.1×10^5 counts. Fig. 4(*a*) summarizes the results of the fraction of counted photons, as defined in §2.3.1. This fraction is plotted *versus* the energy of the incident beam for different values of false counts per pixel per second due to the electronic noise. This plot clearly shows a trade-off between good noise rejection and high detection

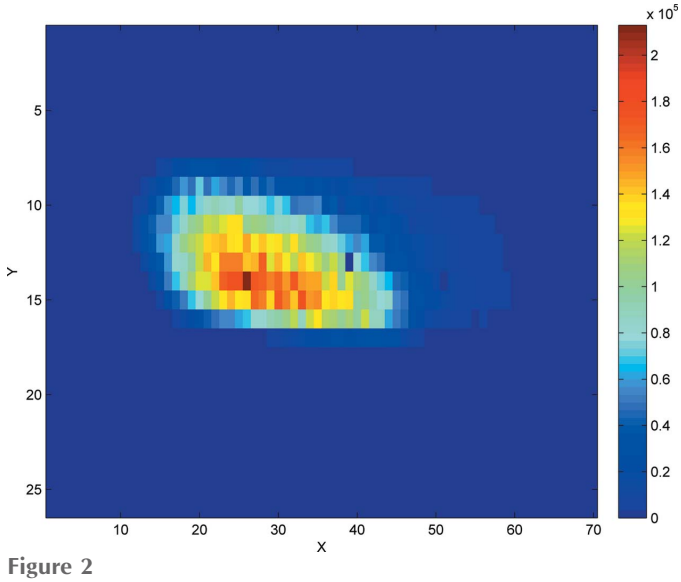

Figure 2
Image of the SXS beam with 2 keV photons using a threshold of 2.2 keV. Medipix3RX is configured in single-pixel mode and super high gain mode.

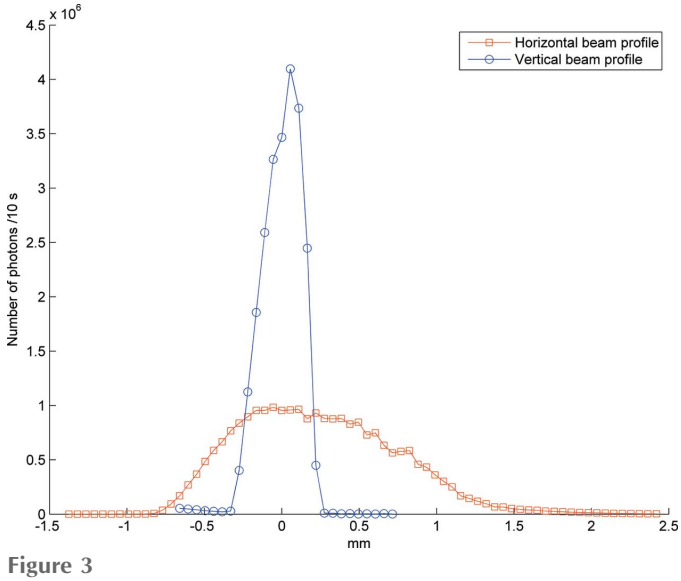

Figure 3
Vertical and horizontal integrated profiles of the SXS beam with 2 keV photons using a threshold of 2.2 keV. Medipix3RX is configured in single-pixel mode and super high gain mode.

efficiency. Fig. 4(*b*) shows the energy thresholds corresponding to the noise values of false counts per pixel per second of Fig. 4(*a*).

3.2. Detective quantum efficiency

3.2.1. Determination of DQE parameters. Various energy scans were performed using the single-pixel mode (SPM) and super high gain mode (SHGM) and the charge summing mode (CSM) as described in §2.3.3. We used the SXS beamline for energies up to 5 keV and fluorescent targets irradiated by a conventional X-ray generator (60 mA, 25 kV) for the higher energies. Fig. 5 shows two different energy scans obtained with

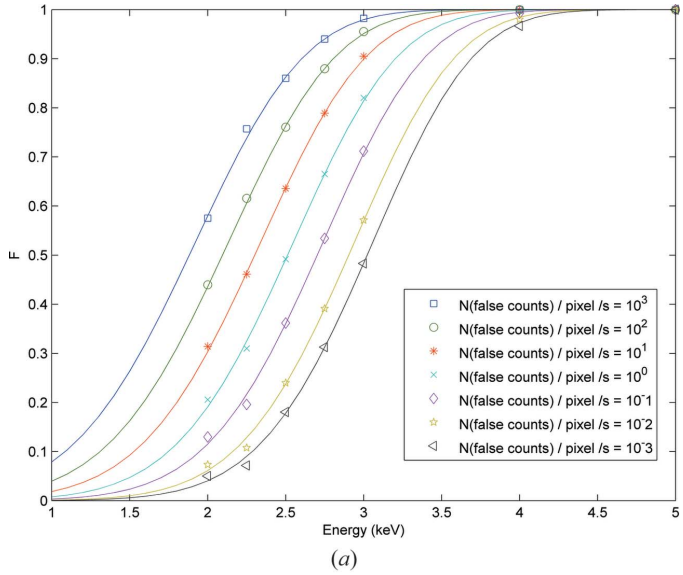

(*a*)

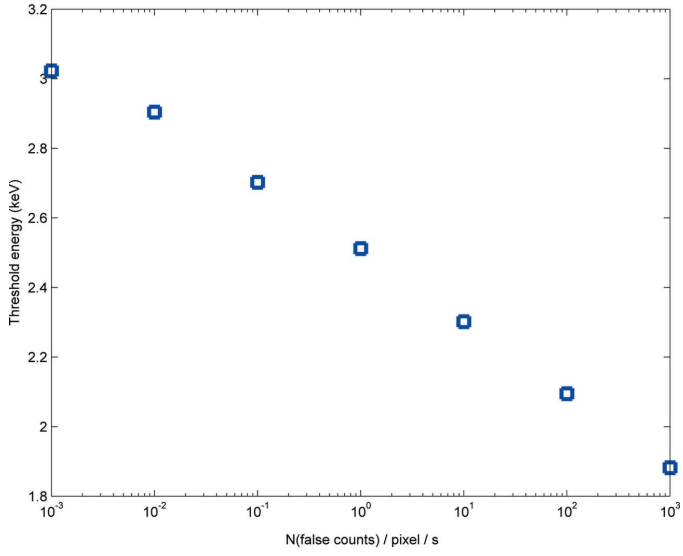

(*b*)

Figure 4
(*a*) Fraction of counted photons as a function of the energy of the incident beam for different values of false counts per pixel and per second due to the electronic noise. (*b*) Energy of the thresholds corresponding to the different values of false counts per pixel and per second due to the electronic noise.

selenium. The curves are fitted by the sum of two Gaussian signals, corresponding to the $K\alpha$ and $K\beta$ emission lines. $K\alpha_1$ and $K\alpha_2$ are approximated by a single monochromatic signal, since the energy resolution of Medipix3RX does not enable the two peaks to be separated. The area under the Gaussian fit of the SPM scan is an estimation of N_1, which is the number of photons that interacted without the charge sharing effect. The area under the Gaussian fit of the CSM scan is an estimation of the incident number of photons multiplied by the sensor efficiency, *i.e.* $N_{\rm in}\, a$.

The probability of charge-sharing is given by equation (15) by comparing N_1 with $N_{\rm in}\, a$. Table 1 shows the values obtained for the different fluorescent targets. This methodology cannot be applied with lower energies since the electronic noise floor corresponds to higher energies in CSM than in SPM with

Table 1
Estimated absorbed number of photons, $N_{in}\,a$, number of photons which interacted without the charge-sharing effect, N_1, and probability of charge-sharing, P, for the different fluorescent targets.

Fluorescent target	K shell emission lines (keV)					
	$K\alpha_1$	$K\alpha_2$	$K\beta_1$	$N_{in}\,a$ (fit CSM)	N_1 (fit SPM)	P
Co	6.930	6.915	7.649	1.5230×10^6	5.6013×10^5	0.6322
Zn	8.639	8.616	9.572	1.6690×10^7	6.3058×10^6	0.6222
Se	11.222	11.181	12.496	2.2773×10^5	8.7182×10^4	0.6172
Zr	15.775	15.691	17.668	1.5658×10^6	5.8188×10^5	0.6284
Ag	22.163	21.990	24.942	3.5686×10^5	1.4373×10^5	0.5972

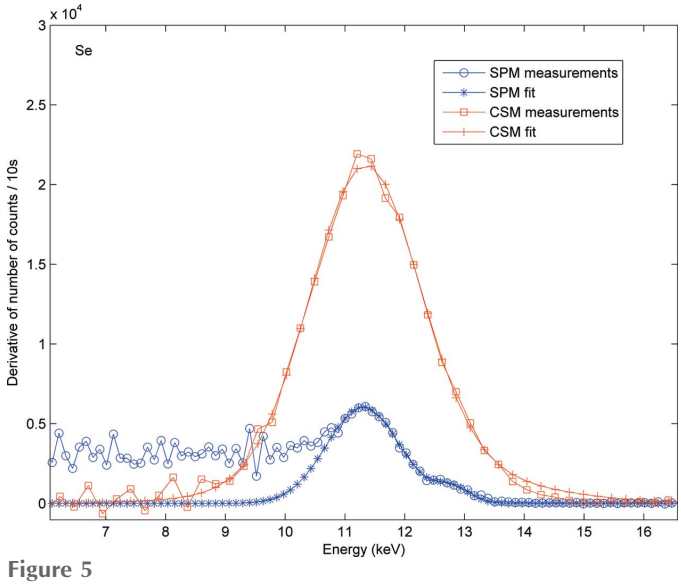

Figure 5
Differential energy scans obtained with a selenium fluorescent target using the single-pixel mode (SPM) and the charge summing mode (CSM). The gain mode for both experiments is set to super high gain mode.

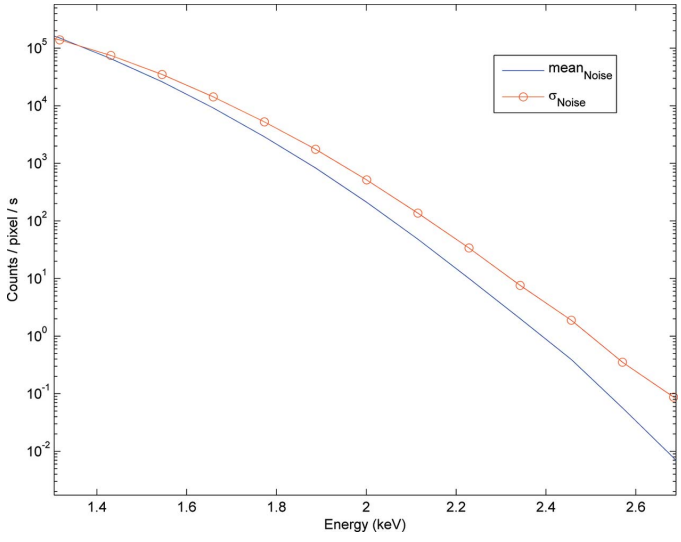

Figure 6
Noise standard deviation, σ_{Noise}, and mean false counts due to electronic noise per pixel, $mean_{Noise}$, in the image as a function of the threshold in single-pixel mode.

SHGM. For the low energies we assume a constant charge-sharing probability, which is given by the mean value of Table 1: $P = 0.619$. A similar result was reported with a different experimental method based on a fit of the threshold scan with an original mathematical model using Medipix3 with a 300 µm-thick Si sensor and 17.4 keV X-rays (Marchal & Medjoubi, 2012). In this paper, the probability of charge sharing was estimated to be $P = 0.64$.

Fig. 6 shows the standard deviation of the noise in the image σ_{Noise} as a function of the threshold in units of keV, using single-pixel mode.

3.2.2. DQE. The detective quantum efficiency at zero spatial frequency was calculated as a function of the threshold and the number of incident photons per pixel and per second, N_{in}, for each measured incident energy.

In SPM combined with SHGM, the analogical dead-time has been previously characterized (Frojdh *et al.*, 2014; Rinkel *et al.*, 2014), giving a mean dead-time value of 0.69 µs. Under these conditions and for a counting rate up to 10^4 photons $pixel^{-1}\ s^{-1}$, the incoming photon flux is well within the linear regime.

We used equations (13) and (16) and the parameters determined in §3.2.1. Figs. 7(*a*) and 7(*b*) show the DQE functions for 4 keV and 11.2 keV incident photons, respectively. For 4 keV photons, the threshold optimizing the DQE clearly depends on N_{in}. When the number of incident photons increases, the threshold energy optimizing the DQE value decreases, resulting in a better optimal DQE. Fig. 8 shows the optimal DQE value as a function of the incident energy and for different numbers of incident photons. For photons with energies higher than 7 keV, the DQE does not depend on the number of photons. Actually, since the DQE optimization is performed within the range $[E_0/2,\ E_0]$, the influence of the electronic noise becomes negligible and the term N_{in} disappears in equation (13), getting back to the classical expression of DQE (Michel *et al.*, 2006).

4. Discussion

The proposed model and associated methodology enables the optimal DQE at zero spatial frequency to be estimated as a function of the X-ray energy. It is based on the calculation of the probability of charge-sharing, among other parameters. In approximation we consider that this probability is constant with energy. Actually, this calculation is not possible for energies lower than 5 keV since the charge summing mode of Medipix3RX does not present such a good separation between X-rays and electronic noise as the single-pixel mode does. The lowest energy at which we could measure this probability was 6.930 keV. We could expect an increasing probability of charge-sharing with lower energies since the mean depth of interaction within the sensor is becoming

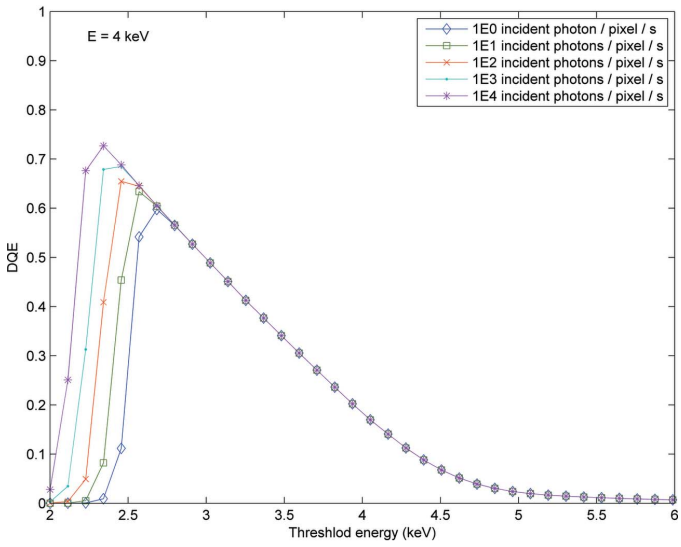

(*a*)

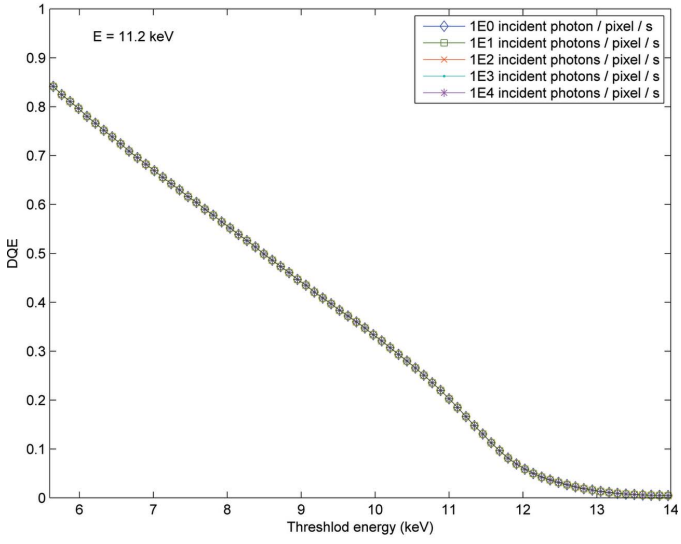

(*b*)

Figure 7
DQE for 4 keV (*a*) and 11.2 keV (*b*) incident photons as a function of the energy threshold for values higher than $E_0/2$ and for different numbers of incident photons pixel^{-1} s^{-1}.

smaller. This mean free path of X-rays within the sensor is estimated by $l = \mu^{-1}$, where μ is the linear attenuation coefficient of X-rays. For 6.930 keV photons interacting with silicon, we find $l = 46$ µm. Since the interactions tend to occur close to the 300 µm sensor surface for 6.930 keV, we assumed similar values of probability of charge sharing for lower energies. The results obtained with soft X-rays were coherent with already published results at 17.4 keV with an underestimation of 3%.

We decided to compare DQE by keeping an event multiplicity of 1. This is justified by the objective of comparing image quality keeping the optimal spatial resolution, which is a key parameter for most applications. Another possibility would be to calculate the multiplicity for energies lower than half the energy of the incident beam and to follow the methodology proposed by Michel *et al.* (2006).

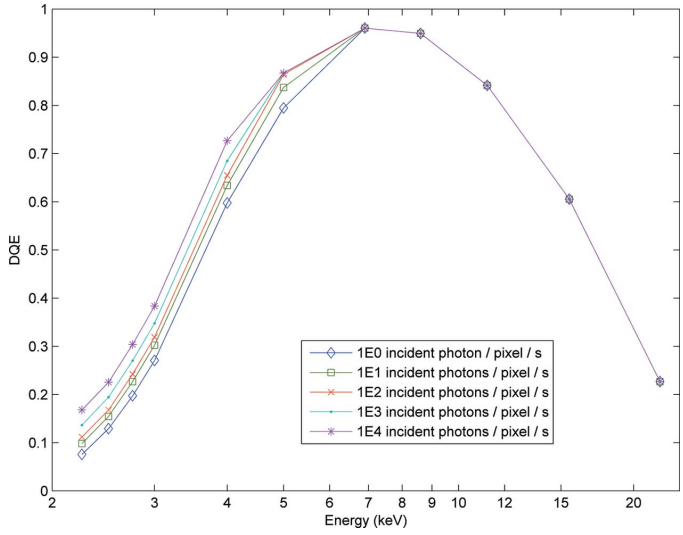

Figure 8
Optimal DQE as a function of the incident energy for different numbers of incident photons pixel^{-1} s^{-1}.

5. Conclusion

We have developed a mathematical model and an associated procedure to determine its parameters for estimating the fraction of counted photons and the detective quantum efficiency at zero spatial frequency in the tender X-ray range for photon-counting detectors. The experiments were carried out with a Medipix3RX ASIC bump-bonded to a 300 µm silicon sensor at the Soft X-ray Spectroscopy beamline (D04A-SXS) at the Brazilian Synchrotron Light Laboratory (LNLS, Campinas, Brazil).

The results presented in this paper set conditions for new possible modalities of X-ray imaging with tender X-ray and photon-counting detectors. Some advantages of soft X-ray imaging can already be identified; for example, higher X-ray fluxes from the synchrotron, higher coherent areas and better speckle resolution for coherent diffraction techniques, and the possibility to image simultaneously different harmonics of the beam. We have shown that Medipix3RX counting detectors can be used down to 2 keV with a not negligible efficiency, which opens up new possibilities in the tender X-ray imaging techniques.

In the tender X-ray range, the results in terms of efficiency and DQE depend on the energy and the incident flux of photons. The optimal DQE values were found in the 7.9–8.6 keV energy range. Since the DQE deterioration is due to the already characterized absorption efficiency of the sensor for higher energies, the deterioration due to electronic noise for lower energies was quantified. For 3 keV photons and 1×10^4 photons pixel^{-1} s^{-1}, the DQE is comparable with that obtained with 19 keV photons, since it is comparable with that obtained with 21 keV photons for 1 photon pixel^{-1} s^{-1}, resulting in a DQE decrease of a factor 1.4. This factor would be representative of the variability of the image quality for applications like XPCS and CDI, usually presenting a large variation of fluxes within the images.

Acknowledgements

This work was carried out within the Medipix3 collaboration. The authors wish to thank Professor Yves Petroff and Dr Helio Cesar Nogueira Tolentino for critical reviewing of the paper.

References

Abbate, M., Vicentin, F. C., Compagnon-Cailhol, V., Rocha, M. C. & Tolentino, H. (1999). *J. Synchrotron Rad.* **6**, 964–972.
Frojdh, E., Ballabriga, R., Campbell, M., Fiederle, M., Hamann, E., Koenig, T. & Zuber, M. (2014). *J. Instrum.* **9**, C04028.
Gimenez, E. N., Ballabriga, R., Campbell, M., Horswell, I., Llopart, X., Marchal, J. & Turecek, D. (2011). *IEEE Trans. Nucl. Sci.* **58**, 323–332.
Henke, B. L., Gullikson, E. M. & Davis, J. C. (1993). *At. Data Nucl. Data Tables*, **54**, 181–342.
Kraft, P., Bergamaschi, A., Bronnimann, Ch., Dinapoli, R., Eikenberry, E. F., Graafsma, H., Henrich, B., Johnson, I., Kobas, M., Mozzanica, A., Schleputz, C. M. & Schmitt, B. (2009). *IEEE Trans. Nucl. Sci.* **56**, 758–764.
Liu, L., Resende, X. R., Rodrigues, A. R. D., Sá, F. H. & Westfahl, H. (2013). *Synchrotron Radiat. News*, **26**(3), 34–38.
Marchal, J. & Medjoubi, K. (2012). *J. Instrum.* **7**, P11028.
Miao, J., Ishikawa, T., Robinson, I. K. & Murnane, M. M. (2015). *Science*, **348**, 530–535.
Michel, T., Anton, G., Böhnel, M., Durst, J., Firsching, M., Korn,, Kreisler, B., Loehr, A., Nachtrab, F., Niederlöhner, D., Sukowski, F. & Takoukam Talla, P. (2006). *Nucl. Instrum. Methods Phys. Res. A*, **568**, 799–802.
Pangaud, P., Basolo, S., Boudet, N., Berar, J. F., Chantepie, B., Clemens, J. C., Delpierre, P., Dinkespiler, B., Medjoubi, K., Hustache, S., Menouni, M. & Morel, C. (2008). *Nucl. Instrum. Methods Phys. Res. A*, **591**, 159–162.
Pennicard, D., Ballabriga, R., Llopart, X., Campbell, M. & Graafsma, H. (2011). *Nucl. Instrum. Methods Phys. Res. A*, **636**, 74–81.
Ponchut, C. (2006). *J. Synchrotron Rad.* **13**, 195–203.
Rinkel, J., Magalhães, D. & Miqueles, E. (2014). *Proceedings of the Third Technology and Instrumentation in Particle Physics Conference (TIPP2014)*, 2–6 June 2014, Amsterdam, The Netherlands. PoS(TIPP2014)212.
Shpyrko, O. G. (2014). *J. Synchrotron Rad.* **21**, 1057–1064.
Van der Veen, F. & Pfeiffer, F. (2004). *J. Phys. Conden. Matter*, **16**, 5003.
Vykydal, Z., Jakubek, J. & Pospisil, S. (2006). *Nucl. Instrum. Methods Phys. Res. A*, **563**, 112–115.
Wang, Z., Gao, K., Chen, J., Hong, Y., Ge, X., Wang, D., Pan, Z., Zhu, P., Yun, W., Jacobsen, C. & Wu, Z. (2013). *Biotechnol. Adv.* **31**, 387–392.
Wernecke, J., Gollwitzer, C., Müller, P. & Krumrey, M. (2014). *J. Synchrotron Rad.* **21**, 529–536.